Remote methane sensing using single-photon PPLN-waveguide upconversion lidar

RUARIDH SMITH, 1,2,* D ARTHUR C. CARDOSO, 3,4 D IMOGEN MORLAND, 1 JACK W. THOMAS, 1 KRISH PANDIYAN, 5 GREG BLANCHARD-EMMERSON, CORIN GAWITH, 5,6 D SARA CARVER, ANDREW WELD, XIAO AI, JOHN G. RARITY, AND LOYD J. McKnight^{1,8}

Abstract: We report on a sensitive methane gas detection system using waveguide-based singlephoton upconversion from 1651 nm to 798 nm wavelength for efficient detection. Single-photon light detection and ranging (LIDAR) techniques offer a route to high-sensitivity direct detection, which is important for environmental monitoring in industrial settings. We report on waveguide fabrication, testing, and overall system development using a fibre-pigtailed waveguide package. We achieve an internal upconversion efficiency of 86%. By combining this system with an active imaging module, we demonstrate methane gas sensing in an outdoor environment. We show this approach is a practical route to enhance the sensitivity of cost-effective environmental monitoring systems.

Published by Optica Publishing Group under the terms of the Creative Commons Attribution 4.0 License. Further distribution of this work must maintain attribution to the author(s) and the published article's title, journal citation, and DOI.

1. Introduction

Deployable solutions for the detection of greenhouse gases are critical for environmental monitoring in industrial settings [1]. A US study showed that industry methane emissions are three times higher than government estimates with considerable environmental and financial implications [2]. Therefore, a comprehensive approach to detection is required to fully quantify these emissions. Current detection methods range from direct measurement at source to satellite-based remote sensing [3].

Single-photon LIDAR techniques offer a route to high sensitivity direct detection [4]. Many greenhouse gas molecules, such as methane, have fundamental absorption lines in the mid-infrared (MIR) spectral region with overtones in the short-wave infrared (SWIR). However, options for efficient single-photon detectors in these wavelength ranges are limited. Superconducting nanowire detectors (SNSPDs) [5], require sizeable cryogenic cooling systems which make them unsuitable for many field-based applications. InGaAs single-photon avalanche diode (SPAD) detectors are widely used in SWIR sensing, yet compared to their near-infrared (NIR)

 $^{^{}I}$ Fraunhofer Centre for Applied Photonics, Fraunhofer UK Research Ltd., Technology and Innovation Centre, 99 George St., Glasgow G1 1RD, Scotland, UK

²School of Engineering, University of Glasgow, Glasgow G12 8QQ, Scotland, UK

³Dept. of Electrical and Electronic Engineering, University of Bristol, Merchant Venturers Building, Woodland Rd., Bristol BS8 1UB, England, UK

⁴Danish Fundamental Metrology, Kogle Allé 5, 2970 Hørsholm, Denmark

⁵Covesion Ltd., Unit F3, Adanac North, Adanac Dr., Nursling, Southampton SO16 0BT, England, UK

 $^{^6}$ Optoelectronics Research Centre, University of Southampton, Southampton SO17 1BJ, England, UK

⁷QLM Technology Ltd., 470 Bath Rd., Arnos Vale, Bristol BS4 3AP, England, UK

⁸Institute of Photonics, University of Strathclyde, 99 George St., Glasgow G1 1RD, Scotland, UK *ruaridh.smith@fraunhofer.co.uk

silicon-based counterparts, suffer in terms of detection efficiency, dark counts and operating temperatures [6,7].

Frequency upconversion, where target infrared photons are converted to shorter wavelengths by the process of sum-frequency generation (SFG), offers a route to sensing at greenhouse gas emission lines across the infrared spectrum. Using this method, detection can be performed at wavelengths where there are commercially available high-efficiency silicon SPADs [8]. These detection schemes are performed in either bulk nonlinear crystals [9] or waveguide geometries [10]. Compared to bulk crystal processes, waveguides offer the potential for high conversion efficiency in single-pass configurations due to tight confinement over extended lengths [11].

Here we present work on magnesium-doped periodically-poled lithium niobate (MgO:PPLN) ridge waveguides, which support good overlapping of confined beams for efficient conversion and strong damage resistance [12,13]. PPLN is a material with high $\chi^{(2)}$ nonlinearity and MgO-doped waveguides have previously demonstrated high conversion efficiencies for second-harmonic generation [14]. Other fabrication methods include Ti-indiffused and reverse proton exchange (RPE) waveguides, with ridge waveguides chosen here for their favourable power handling [15]. We have fabricated MgO:PPLN ridge waveguides for the upconversion of light at the methane gas line of 1651 nm to NIR wavelengths for detection. The 1651 nm gas line is chosen for it's strong absorption and low interference from other atmospheric gases [16].

Applying upconversion to remote greenhouse gas sensing is a field of great interest [17,18]. Previous works have combined upconversion detection to widely used remote optical sensing techniques such as integrated path differential absorption (IPDA) lidar and differential absorption lidar (DIAL) [19,20]. Our measurements were performed using QLM Technology Ltd.'s patented lidar absorption spectroscopy technique, known as TDLidar [21]. This technique combines attributes of tuneable diode laser absorption spectroscopy (TDLAS) [22] and DIAL [23] with time-correlated single-photon counting (TCSPC). The method aims to increase the range of traditional TDLAS systems with sensitive single-photon detection whilst offering a more compact and cost-effective solution for continuous industrial monitoring than DIAL [24].

In this work we first report on the waveguide fabrication process in Section 2. In Section 3 we detail initial upconversion tests and detection efficiencies from free-space waveguide testing and the fibre-packaged waveguide. We then demonstrate the potential of this technology in Section 4 by deploying a combined upconversion module, containing a fibre-packaged PPLN waveguide and SPAD, with an active imaging module to detect methane gas.

2. Waveguide fabrication

The MgO:PPLN ridge waveguides used in this work were manufactured by Covesion Ltd using the approach reported in Refs. [14,25] and illustrated in Fig. 1(a). Fabrication is based on three successive stages of zinc indiffusion to create a planar guiding layer, ultra-precision machining into the planar layer to form ridge waveguides, and preparation of angle cut optical facets by ductile dicing, a process that we have previously demonstrated to achieve 0.3 nm surface roughness in lithium niobate [26]. The devices described in this paper were prepared in 1 mm-thick 5% MgO:PPLN wafers each containing multiple 1.2 mm-wide 19.72 µm period gratings designed to access Type-0 1651+1543 \rightarrow 798 nm SFG at 40°C via the d_{33} nonlinear coefficient. 100 nm of metallic zinc was sputtered onto the +z surface of the MgO:PPLN wafer using an Oxford Instruments Plasma Lab System 400 and indiffused at 950°C in an oxygen atmosphere to promote ZnO formation. To facilitate high pump and SHG modal overlap at our chosen wavelengths, five ridge widths were cut into each PPLN grating ranging from 11-13 µm in 0.5 µm steps and parallel to the [100] x-direction of the crystal. These fabrication parameters were chosen based on our previous work and optimisation of MgO:PPLN ridge waveguides for 1560 nm SHG [25]. An example SEM image of a ridge waveguide facet is shown in Fig. 1(b) to illustrate the uniformity of dicing. Individual chips measuring 40 mm-long by 5 mm-wide were singulated from the wafer

and the optical facets prepared using ductile dicing. Finally, the input and output facets of each chip were broadband anti-reflection (AR) coated around the three SFG wavelengths of interest.

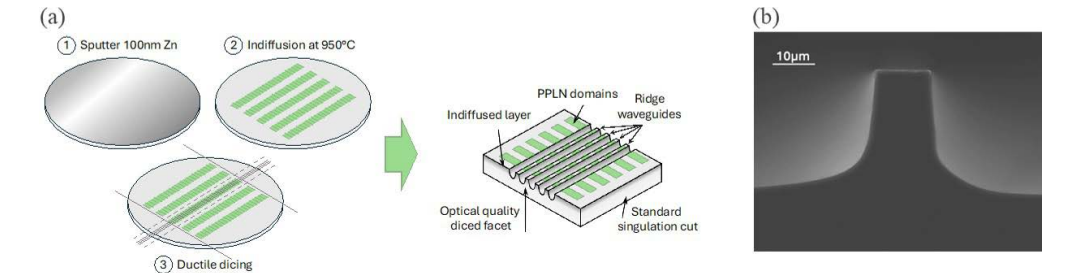


Fig. 1. (a) Fabrication of diced ridge PPLN waveguides by (1) deposition of 100 nm metallic zinc layer onto a PPLN wafer, (2) indiffusion of metallic zinc at 950° C in an O_2 atmosphere to create a planar guiding layer, (3) ductile dicing of optical quality ridge waveguides and facets. The resulting ridge waveguide chip structure is also shown. (b) SEM image of $13 \, \mu \text{m}$ -wide MgO:PPLN ridge waveguide facet by ductile dicing.

3. Optical tests

3.1. Free-space coupled waveguide upconversion results

A PPLN ridge waveguide chip was integrated into an upconverison detection system for free-space characterisation with continuous-wave (CW) sources as shown in Fig. 2. A 1651 nm DFB laser (Applied Optoelectronics, Inc.) was combined with an amplified 1550 nm tuneable laser source (Santec TSL-550) inside a custom wavelength division multiplexer (WDM) (OZ Optics Ltd.). In this work we define the light from the 1651 nm laser as the signal, the high power tuneable 1550 nm source as the pump and the generated shorter-wavelength light at 798 nm as the upconverted light. A free-space section was included before coupling into the waveguide to allow additional polarisation control with half-wave plates and narrow bandpass filters to block broadband background light from the amplifier prior to launch into the waveguide. The combined beams were coupled into the waveguide via a zoom collimator and 15.3 mm focal length coupling lens. The output light of the waveguide was collimated with another 15.3 mm focal length lens, and the three wavelengths split into separate beam paths via dichroic mirrors for independent detection. An additional narrow 808 nm bandpass filter (FWHM = 3 nm) was placed in the upconversion beam arm and angle tuned to filter out any unwanted wavelengths whilst still allowing the upconverted light to be detected on a calibrated Thorlabs photodetector.

Maximium upconversion occurs in the PPLN waveguide when the quasi-phase matching conditions are met [27]. For $\chi^{(2)}$ nonlinearities this requires the wavevector mismatch factor, Δk , to be satisfied according to the equation,

$$\Delta k = k_s + k_p - k_{up} - 2\pi/\Lambda = 0, \tag{1}$$

where k_i (i = s, p, up) are the wavevectors for the signal, pump and upconverted beams respectively and Λ is the poling period of the crystal. Deviation from perfect phase-matching conditions results in a decrease in the efficiency of the conversion process for a waveguide of length L in the presence of a strong pump P_p according to the equation,

$$\eta(\Delta k) = \eta_{nor} P_p L^2 sinc^2 \left(\frac{\Delta k L}{2}\right),\tag{2}$$

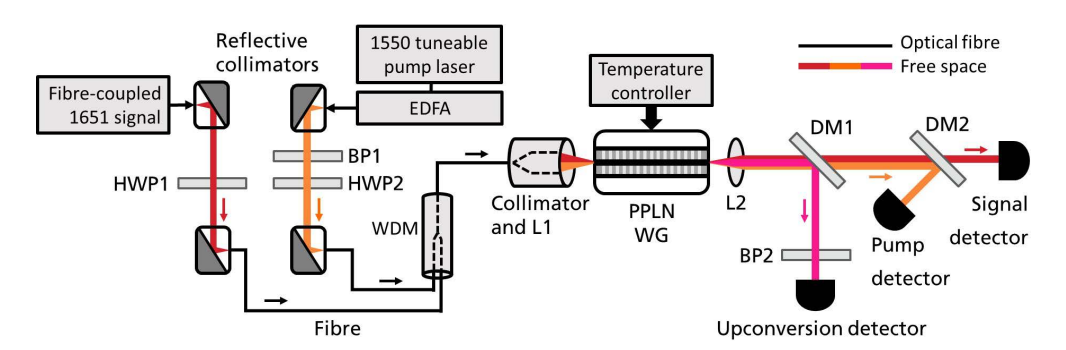


Fig. 2. Waveguide test set-up for upconversion characterisation. HWP1: half-wave plate @ 1650 nm , HWP2: half-wave plate @ 1550 nm, BP1: 1550 nm bandpass filter, BP2: 808 nm bandpass filter, DM1: dichroic mirror (HR @ 800 nm; HT @ 1550, 1650 nm), DM2: dichroic mirror (HR @ 1550 nm; HT @1650 nm) WDM: wavelength division multiplexer, EDFA: erbium-doped fibre amplifier, L1,2: 15.3 mm fl. lens, Fibre: single-mode polarisation-maintaining fibre, WG: mounted PPLN waveguide chip.

with the normalised conversion efficiency η_{nor} [15] given by the equation,

$$\eta_{nor} = \frac{1}{A_{eff}} \left(\frac{8\pi^2 \nu_s \nu_{up} d_{eff}^2}{n_s n_p n_{up} c^3 \epsilon_0} \right),\tag{3}$$

where v_s and v_{up} are the signal and upconverted frequencies, c is the speed of light in vacuum, ϵ_0 is the vacuum permittivity, d_{eff} is the effective nonlinear coefficient and n_i (i = up, p, s) are the refractive indices at the corresponding wavelengths. The refractive index for MgO-doped congruent LiNbO3 is derived from literature [28] and the effective refractive indices of the modes are computed using the commercial software FIMMWAVE. A_{eff} is the effective modal area of the waveguide taking into account the spatial overlap of the interacting beams. Fig. 3(a) shows the phase-matching conditions for the upconverted light generated in a 13 µm wide PPLN ridge waveguide. The waveguide is temperature stabilised at 40°C with an oven. The maximum upconversion efficiency is detected for a pump wavelength of 1543.7 nm and a signal of 1651 nm. The corresponding upconverted wavelength is 798 nm and the pump spectral acceptance bandwidth is 0.62 nm (2.60 cm⁻¹). A slight variation between measured data and the theoretical sinc² fit is caused by variations in the quasi-phase matching conditions during fabrication [29]. Inset shows the mode profile of the unconverted beam which is experimentally measured to have a $1/e^2$ mode size of 10.33 x 6.09 µm.

Figure 3(b) shows the upconverted power as a function of the transmitted pump power for 3 different signal powers measured at 40°C. For a transmitted signal power of 3.9 mW (black line) the maximum upconverted power recorded is 6.96 mW. To calculate the upconversion efficiency, the energy ratio between the longer-wavelength signal photons and shorter-wavelength upconverted photons is taken into account, as we define the upconversion efficiency as,

Upconversion Efficiency =
$$\frac{P_{up}\lambda_{up}}{P_s\lambda_s} = \frac{N_{up}(L)}{N_s(0)}$$
, (4)

where P_i (i = up, s) and λ_i (i = up, s) are the powers and wavelengths of the upconverted and signal beams respectively, which relates to the number of upconverted photons generated after the waveguide $N_{up}(L)$ as a function of the number of signal photons transmitted with no pump applied $N_s(0)$. Using this formula, we calculate the maximum internal upconversion efficiencies for input signal powers of 3.9 mW, 2.6 mW and 1.5 mW to be 86.2%, 81.7% and 79.5% respectively.

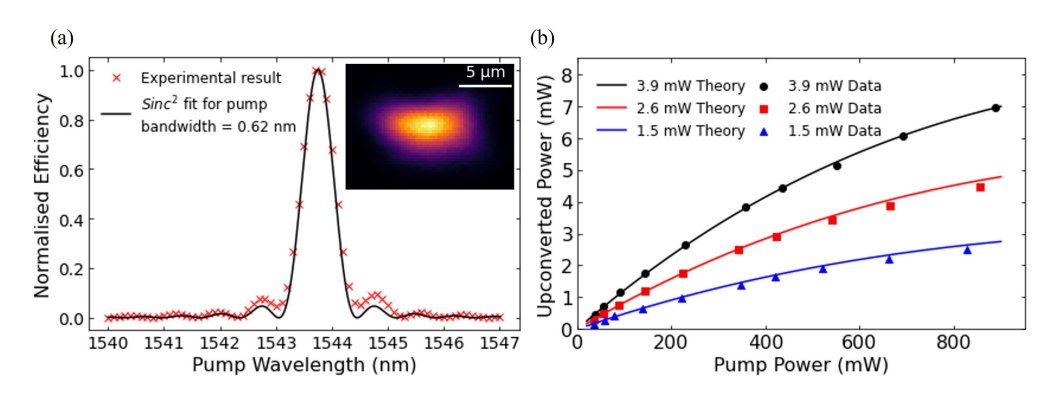


Fig. 3. (a) Upconversion phase-matching spectrum as a function of pump wavelength with inset showing the upconverted mode profile. (b) Upconversion free-space coupled results plotted as a function upconverted power agianst pump power for 3 different input signal powers.

We define this as internal efficiency as this does not include waveguide coupling efficiency. Due to the high efficiency of the conversion process we also consider the depletion of the the pump [30]. In this case the evolution of upconverted power with signal and pump depletion is given by the expression,

$$P_{up} = P_s \frac{\lambda_s + \lambda_p}{\lambda_p} sn^2 \left(\sqrt{\eta_{up} P_p \frac{\lambda_p}{\lambda_s + \lambda_p}} \left| \frac{P_s \lambda_s}{P_p \lambda_p} \right|,$$
 (5)

where P_i (i = up, p, s) and λ_i (i = up, p, s) are the powers and wavelengths of the upconverted, pump and signal beams respectively. In the case of pump depletion, the relationship between the upconversion efficiency η_{up} and the normalised conversion efficiency η_{nor} described in Eq. (3) is given by $\eta_{up} = \eta_{nor}L^2$. The theoretical upconversion power against transmitted pump power is shown above in Fig. 3(b). The conversion efficiency is consistent across the three power levels and still increasing with pump power, indicating a maximum efficiency still to be reached.

3.2. Fibre-packaged PPLN waveguide upconversion results

For the gas sensing demonstration, a PPLN waveguide was fibre-packaged by Covesion Ltd with standard PM1550 and PM850 input and output fibres respectively, along with an integrated TEC. Single-photon upconversion counts (blue line) and noise count rate (green line) are plotted against input pump power for the waveguide package using an attenuated source of 1651 nm photons as shown in Fig. 4. The upconversion module setup is shown in Fig. 5. Calibrated ND filters attenuate a 1651 nm DFB laser source to the single-photon level which combines with a pump laser source at 1547 nm (wavelength tuned to the phase matching peak for this new chip) inside a WDM. The output of the WDM is then fibre coupled into the waveguide package temperature controlled at 40°C. The light at the output of the fibre package is collimated and filtered using a narrow bandpass filter before the upconverted photons at 799 nm are fibre-coupled and detected on an Excelitas SPAD (SPCM-AQRH-16-FC).

Based on the calibration of the ND filters, the maximum predicted number of signal photons is 130 MHz (130 million counts per second). We experimentally measured upconversion counts of 4.50 MHz for an input pump power of 932 mW with noise counts of 7.04 MHz. This corresponds to an overall upconversion module single-photon detection efficiency of 3.47%. This value includes all losses in the system such as losses associated with the coupling of the two sources into the waveguide, the conversion efficiency of the waveguide, losses from the output fibre alignment, collection optics and SPAD efficiency.

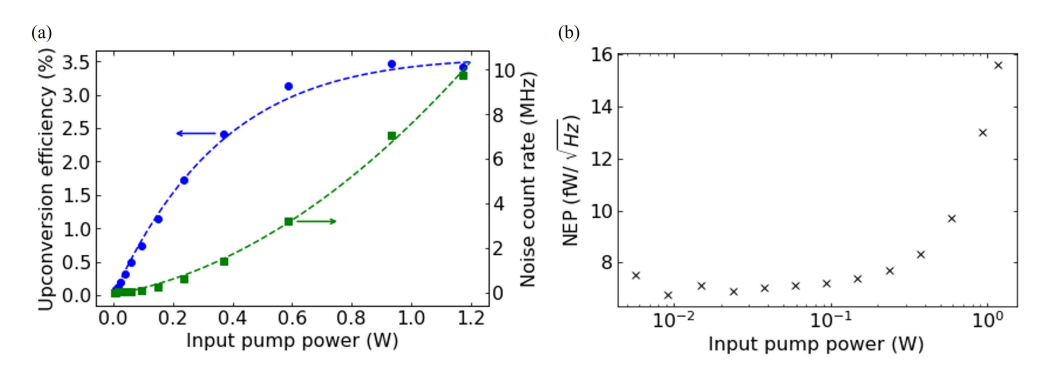


Fig. 4. (a) Single-photon upconversion efficiency of waveguide package (blue) fitted to Eq. (5) (blue dash) and noise count rate counts detected with only pump light launched into to waveguide (green) with polynomial fit (green dashed). (b) Upconversion NEP as an evolution of input pump power based on the results shown in Fig. 4(a).

The right-hand axis (green dashed line) in Fig. 4(a) shows the evolution of noise counts with increasing pump power. These counts are obtained when only the pump light is launched into the fibre. As previously reported, the origin of this background noise is likely dominated by parasitic nonlinear processes occurring in the waveguide [15]. Potential broadband SPDC (Spontaneous Parametric Down Conversion) noise generated in the waveguide is subsequently upconverted at our detection wavelength which cannot be filtered out [31,32]. Fibre coupling and narrow bandpass filters are used to reduce this noise, however a significant amount remains detectable due to the overlap with our upconverted wavelength. This noise ultimately limits the signal-to-noise ratio of the detection system.

Figure 4(b) plots the common figure of merit for sensitivity of our upconversion detector known as the noise-equivalent power (NEP) [31], given by the equation,

$$NEP = \frac{hv_s}{DE} \sqrt{2NCR} \tag{6}$$

where DE is the detection efficiency of the combined waveguide and SPAD system, and NCR is the noise count rate which includes the detector dark count and pump background noise. Expressed as a function of the signal frequency, v_s , the NEP of the system at maximum overall detection efficiency (3.47%) is 13.0 fW/ $\sqrt{\text{Hz}}$. This reflects a large background noise contribution from the pump.

4. Remote methane sensing

For the methane sensing demonstration, the upconversion module described above was combined with an imaging module as shown in Fig. 5. The transceiver module first transmits the 1651 nm signal laser through a gas cell and beam splitter (BS) before being directed at the target gas cloud via a telescope. The gas cloud was illuminated with 10 mW of light with the scattered light collected at the receiver through the reflected port of the beam splitter. After being coupled into a fibre, the back-scattered light was sent to the upconversion module containing the fibre-pigtailed PPLN waveguide package. Here the collected light was combined with the amplified pump laser source in the WDM and coupled to the packaged PPLN waveguide, generating upconverted light at 799 nm. The angle tuned 808 nm bandpass filter (BP2) was used to block background light from the pump laser and probe (collected scatter), with the upconverted light detected on the SPAD.

The telescope is designed to collimate and expand light from a fibre-coupled laser diode with a pair of 7.5 mm focal length aspheric lenses. The expanded beam is then launched through a set of

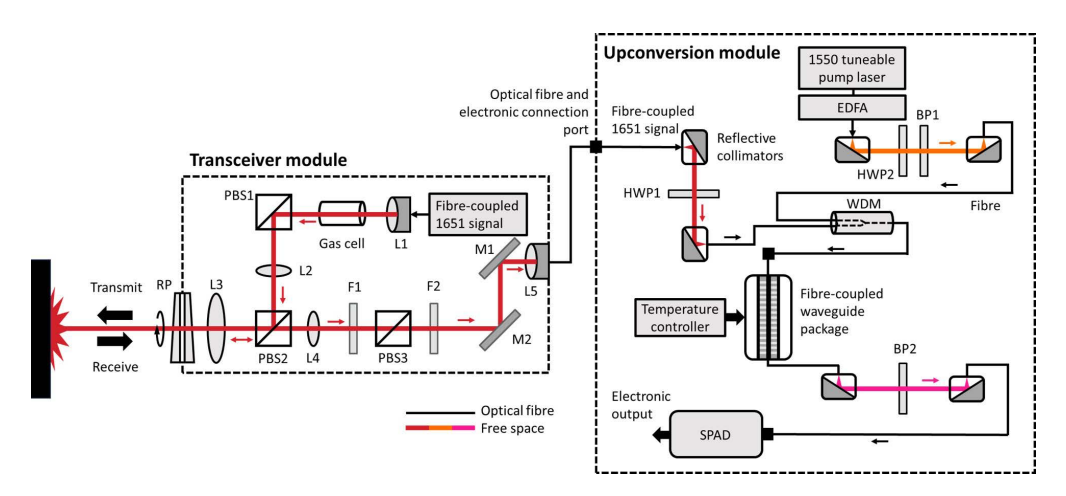


Fig. 5. Experimental setup used for the methane sensor based on upconversion of light. A probing laser beam (1651 nm) is launched from the transceiver, passes through a gas plume and is backscattered from a solid target. The returning light is collected into an optical fibre, led to a wavelength division multiplexer (WDM) and merged with a pump laser (1547 nm). The two modes combine in a PPLN waveguide, where they are upconverted to near-infrared photons (799 nm). A bandpass filter centred on this wavelength blocks the short wave infrared light and the mode generated by upconversion is detected by a silicon photon counting detector. Lx: lenses, RP: Risley prisms, PBSx: polarisation beamsplitter, Fx: filters, Mx: protected silver mirror, HWPx: half-wave plate, BPx: bandpass filter.

Risley prisms via a main 50 mm diameter lens with a 150 mm focal length. Backscattered light is collected through the same main lens and fibre-coupled via another pair of aspheric lenses. Polarisation beam splitters (PBS) are used to split the transmit and receive arms of the telescope. This design allows us to adjust the focal length of the probing beam and increase the number of photons collected by either focusing the laser on the target for close distances or collimating the light for longer-range applications. The Risley prisms allow for beam steering and enable an image of the whole scene to be acquired to precisely locate methane gas plumes.

As mentioned in Section 1, methane detection measurements were performed using QLM Technology Ltd.'s patented lidar absorption spectroscopy technique, known as TDLidar [21]. TDLidar involves rapidly tuning the wavelength of the probing laser around methane's absorption line at 1650.9 nm at a rate of approximately 1 MHz [33]. The returned photon count is sampled at discrete time intervals as the wavelength sweeps up and down in frequency spanning the absorption peak. Multiple spectral measurements are then averaged and the absorption line spectral fit made to determine the strength of the methane absorption relative to an internal gas reference cell, using the absorption cross-section value obtained from the HITRAN database [34].

The averaged spectral data is output at a rate of 100 Hz, a 10 ms measurement time for each pixel in the image scan. After upconversion photon count rates of 2 MHz were detected (2000 counts per measurement time). The average methane concentration along the observation path-length is then determined using the distance information from the lidar signal. Pulses of light are launched such that the time of flight (TOF) enables calculation of the distance from the backscattering target. The probing laser amplitude is additionally modulated with a pseudo-random bit sequence for enhanced signal-to-noise. The upconversion process and time-domain sampling maintains the spectral information such that the frequency sweep of the infrared light is transferred to the upconverted 798 nm signal, enabling the spectral intensity at 1651 nm to be measured from the number of photons counted by the silicon SPAD.



Fig. 6. Methane sensing results. Top (left) picture taken from the gas cell inside the lab and image produced from the laser scan (right) of the scene with the methane concentration map. The bottom (left) picture from the gas cell located in an outdoor environment and the methane concentration path length image obtained from the probing laser scan, with light traversing the gas cell being scattered off the background wall at a range of 25 m.

The pictures taken from the scene and the images obtained from the laser scan are shown in Fig. 6. The top line shows the picture taken from the gas cell in the laboratory (left) and an image with the methane concentration distribution mapped with the presented method (right) by the probing laser scan. The acquisition time for each image was 180 seconds with an approximate image resolution of 100 x 100 pixels (0.2 degree angular resolution). The TOF data indicate that the background is around 8 m away. For the second round of measurements (bottom line of Fig. 6) we put the gas cell outdoors to mimic a real application scenario where the system can be used. A picture of the landscape is shown (left) as well as the image obtained from the laser scan (right). By collecting light backscattered from the background around 25 m away we could image and detect the gas cell. The path length through the methane absorption cell (2.5% gas concentration at ambient pressure) is 25 cm with an absorption cross-section value of $1.8 \times 10^{-24} \text{m}^2 \cdot \text{mol}^{-1}$ at the probing wavelength. The width of each scan is 120 pm, taken every 1 µs then integrated for 10 ms to calculate a path-integrated concentration. Methane concentrations of 1000 ppm·m were readily detected at 25 m. The missing return photons from the building behind in the top right of this image indicates a range limit of around 40 m for this current system. QLM Technology Ltd. have previously demonstrated methane leak detection over a range of at least 90 m with a comparable system using an InGaAs SPAD detector [33]. The range limitation of the system is linked to the coupling inefficiencies of fibre-packaged waveguide design. Incremental efficiency

improvements such as those demonstrated in our free-space system, and further noise suppression methods, present a path to performance enhancement over InGaAs-based systems.

Discussions and conclusion

5.1. Comparison to state-of-the-art

In this work we achieve 1651 nm upconversion with internal conversion efficiencies of up to 86% in free-space PPLN waveguide testing. We further report an overall system single-photon efficiency (including all coupling losses, internal upconversion efficiency and SPAD detector efficiency) of 3.5% in our fibre-package system with a noise count rate of 7 MHz. The main comparison to be made with this detection scheme is with InGaAs detector-based systems. State-of-the-art photon detection efficiencies of InGaAs SPADs are capable of reaching over 50% at 1550 nm [35], with commercial InGAas detectors achieving 25% efficiency with dark count rates of around 1 kHz at 1550 nm [36]. InGaAs performance is typically lower at 1651 nm, with recent works reporting device operating around 5% [33,37]. We surpass this performance on bench but not yet in a packaged module, demonstrating upconversion detection has the potential to offer previously unavailable performance benefits through using silicon SPADs over InGaAs (such as extending the detection range to longer wavelengths). The commercial silicon SPAD used in this work has a peak detection efficiency of over 70% [38] and, once resolvable performance issues in the packaged waveguide are addressed, we hope to be able to combine a higher efficiency upconversion module with these SPADs to compete with the best-in-class systems.

There are a number of different upconversion schemes reported in literature. Previous bulk crystal systems have been developed [9] with many schemes targeting wide-field of view imaging applications [39]. Techniques to increase the conversion efficiency of these systems include resonant cavity designs [40], cascaded crystals [30] and kW-levels of pump power [17]. More recent work has shown high efficiency conversion (30% overall detection efficiency) in bulk crystal with low NEP ($3 \times 10^{-17} \text{ W}/\sqrt{\text{Hz}}$) by using pulsed laser sources. [41]. The waveguide approach has shown conversion efficiencies higher than bulk crystals using continuous-wave pump sources [10,11]. This allows us to reduce the complexity of the system and develop a compact demonstrator for deployable applications.

Promising work in RPE PPLN waveguides report system detection efficiency of 36% with noise counts of 200 Hz by utilising a tapered fiber input combined with on-chip filtering [42]. The waveguides in our paper are based on a ridge waveguide fabrication process. These waveguides are well suited for enabling good overlap of interacting beams, even with wide wavelength separation, and is a favoured geometry for increasing the wavelength of detection, along with high-power handling. Recent work in comparable PPLN ridge waveguides, has reported MIR upconversion at 3.5 μ m with detection efficiencies of 0.4% with dark counts of 22 kHz [15]. Extending detection into the MIR is an area of future work with several papers reporting efficient detection [43,44]. Work in developing thin-film lithium niobate waveguides is also being pursued for integrated photonic platforms, but suffers from challenges in efficient waveguide coupling [45,46].

The benefit of active imaging systems for methane monitoring is that they can capture the source of emission [18]. DIAL systems are capable of highly sensitive measurements at km ranges [24], however the size and cost of many of these systems limit their use for continuous industrial leak detection. Upconversion imaging methods for methane detection have previously been demonstrated in the lab at ranges of 2 m [17] and combined with non-imaging DIAL techniques for atmospheric monitoring at km ranges [19,47]. The upconversion detection system presented in this work represents an adaptation to previous TDLidar work, which uses InGaAs SPADs for remote gas imaging. TDLidar system reports ranges of 90 m and sensitivities down to 100 ppm·m [33], compared to the 1000 ppm·m at 40 m achieved with this system. Improvements

need to be made in order to compete with this and routes have been identified to refine the upconversion module. In the future, upconversion schemes may provide additional benefits such as direct aerosol backscatter imaging without the requirement of hard targets in compact systems and open-up increased sensitivity at MIR wavelengths for new detection capabilities. However, this brings additional challenges such as designing cost-effective collection optics lidar transceiver system and, whilst methane absorption lines are stronger in the MIR, for long-range detection this is not always desirable as total absorption of the laser radiation results in no signal return [16].

Overall, our approach to nonlinear conversion provides a high-reliability high-efficiency route to longer wavelength detection while minimising overall system SWaP.

5.2. Future work

Future work will build on this system to address the challenges mentioned. Through improved fibre-coupling of the waveguide package, we aim to improve the modal overlap of our interacting beams to increase conversion efficiency. With this we hope to replicate the 86% efficiency of our lab-based system in the portable packaged module. We can further decrease background noise by replacing off-the-shelf bandpass filters with custom optics designed to fit the phase-matching bandwidth. Other noise reduction techniques to explore include pulsed pumping schemes [44], using a longer-wavelength pump to decrease parasitic noise [31], spatial filtering and investigating temperature-dependent noise sources [47]. With each scheme there are trade-offs to consider, such as the limited availability of cost-effective, high-power compact longer-wavelength lasers sources (particularly for future commercial and MIR applications).

We are working towards developing compact upconversion modules for longer wavelength detection, for example to target CO_2 absorption lines at 2 µm. This would increase the spectral range of TDLidar beyond current InGaAs systems and open up previously unreachable applications. We have performed initial simulations that indicate that even for very modest upconversion efficiencies a CO_2 sensor using a similar approach can reach a sensitivity better than 1000 ppm·m.

5.3. Conclusion

In this work we have presented a novel approach to direct measurement of greenhouse gases using single-photon upconversion detection. We have demonstrated methane gas detection with concentrations of 1000 ppm·m at a range of 25 m. We achieved this with a fibre-pigtailed PPLN waveguide package. In addition, we achieve an internal upconversion efficiency of up to 86% in free-space waveguide testing. Background noise ultimately limits the signal-to-noise ratio of the detection system, resulting in a high NEP value. This is reflected in the relatively low conversion efficiency of the waveguide package compared to our free-space coupled device. We are currently investigating methods to improve this, such as using custom narrow bandpass filters and pumping at longer-wavelengths than the signal. The approach outlined here is a promising method suitable for the detection of a range of greenhouse gases, where adding a frequency conversion step to TDLidar can extending the range of the current system beyond InGaAs detector ranges. This is the subject of ongoing work.

Funding. Innovate UK (10032211); Royal Academy of Engineering (RCSRF1718639); Engineering and Physical Sciences Research Council (EP/S023321/1).

Disclosures. The authors declare no conflicts of interest.

Data availability. Data underlying the results presented in this paper may be obtained from the authors upon reasonable request.

References

 W. Collins, R. Orbach, M. Bailey, et al., "Monitoring methane emissions from oil and gas operations[‡]," Opt. Express 30(14), 24326–24351 (2022).

- E. D. Sherwin, J. S. Rutherford, Z. Zhang, et al., "US oil and gas system emissions from nearly one million aerial site measurements," Nature 627(8003), 328–334 (2024).
- J. Cooper, L. Dubey, and A. Hawkes, "Methane detection and quantification in the upstream oil and gas sector: the role of satellites in emissions detection, reconciling and reporting," Environ. Sci.: Atmos. 2(1), 9–23 (2022).
- A. McCarthy, G. G. Taylor, J. Garcia-Armenta, et al., "High-resolution long-distance depth imaging LiDAR with ultra-low timing jitter superconducting nanowire single-photon detectors," Optica 12(2), 168–177 (2025).
- I. Esmaeil Zadeh, J. Chang, J. W. N. Los, et al., "Superconducting nanowire single-photon detectors: A perspective on evolution, state-of-the-art, future developments, and applications," Appl. Phys. Lett. 118(19), 190502 (2021).
- R. H. Hadfield, J. Leach, F. Fleming, et al., "Single-photon detection for long-range imaging and sensing," Optica 10(9), 1124–1141 (2023).
- F. Telesca, F. Signorelli, and A. Tosi, "Temperature-dependent photon detection efficiency model for InGaAs/InP SPADs," Opt. Express 30(3), 4504–4514 (2022).
- J. S. Dam, P. Tidemand-Lichtenberg, and C. Pedersen, "Room-temperature mid-infrared single-photon spectral imaging," Nat. Photonics 6(11), 788–793 (2012).
- A. P. Vandevender and P. G. Kwiat, "High efficiency single photon detection via frequency up-conversion," J. Mod. Opt. 51(9-10), 1433–1445 (2004).
- C. Langrock, E. Diamanti, R. V. Roussev, et al., "Highly efficient single-photon detection at communication wavelengths by use of upconversion in reverse-proton-exchanged periodically poled LiNbO₃ waveguides," Opt. Lett. 30(13), 1725–1727 (2005).
- 11. H. Kamada, M. Asobe, T. Honjo, *et al.*, "Efficient and low-noise single-photon detection in 1550 nm communication band by frequency upconversion in periodically poled LiNbO₃ waveguides," Opt. Lett. **33**(7), 639–641 (2008).
- 12. W. M. Young, M. M. Fejer, M. J. F. Digonnet, *et al.*, "Photorefractive-damage-resistant Zn-diffused waveguides in MgO:LiNbO₃," Opt. Lett. **16**(13), 995–997 (1991).
- T. Umeki, O. Tadanaga, and M. Asobe, "Highly Efficient Wavelength Converter Using Direct-Bonded PPZnLN Ridge Waveguide," IEEE J. Quantum Electron. 46(8), 1206–1213 (2010).
- L. G. Carpenter, S. A. Berry, A. C. Gray, et al., "CW demonstration of SHG spectral narrowing in a PPLN waveguide generating 2.5 W at 780 nm," Opt. Express 28(15), 21382–21390 (2020).
- L. Lehmann, L. Grossard, L. Delage, et al., "Single photon MIR upconversion detector at room temperature with a PPLN ridge waveguide," Opt. Express 27(14), 19233–19241 (2019).
- 16. H. Riris, K. Numata, S. Li, et al., "Airborne measurements of atmospheric methane column abundance using a pulsed integrated-path differential absorption lidar," Appl. Opt. **51**(34), 8296–8305 (2012).
- M. Imaki and T. Kobayashi, "Infrared frequency upconverter for high-sensitivity imaging of gas plumes," Opt. Lett. 32(13), 1923–1925 (2007).
- 18. M. Kwaśny and A. Bombalska, "Optical Methods of Methane Detection," Sensors 23(5), 2834 (2023).
- 19. L. Høgstedt, A. Fix, M. Wirth, *et al.*, "Upconversion-based lidar measurements of atmospheric CO₂," Opt. Express **24**(5), 5152–5161 (2016).
- L. Meng, A. Fix, M. Wirth, et al., "Upconversion detector for range-resolved DIAL measurement of atmospheric CH₄," Opt. Express 26(4), 3850–3860 (2018).
- 21. J. Titchener and X. Ai, "Rapidly tuneable diode lidar," GB patent 2586075B (28 July 2021).
- H. I. Schiff, G. I. Mackay, and J. Bechara, "The use of tunable diode laser absorption spectroscopy for atmospheric measurements," Res. Chem. Intermed. 20(3-5), 525–556 (1994).
- R. A. Baumgartner and R. L. Byer, "Continuously tunable ir lidar with applications to remote measurements of SO₂ and CH₄," Appl. Opt. 17(22), 3555–3561 (1978).
- F. Innocenti, R. Robinson, T. Gardiner, et al., "Differential Absorption Lidar (DIAL) Measurements of Landfill Methane Emissions," Remote Sens. 9(9), 953 (2017).
- S. A. Berry, L. G. Carpenter, A. C. Gray, et al., "Zn-indiffused diced ridge waveguides in MgO:PPLN generating 1 watt 780 nm SHG at 70% efficiency," OSA Continuum 2(12), 3456–3464 (2019).
- L. Carpenter, S. Berry, and C. Gawith, "Ductile dicing of LiNbO₃ ridge waveguide facets to achieve 0.29 nm surface roughness in single process step," Electron. Lett. 53(25), 1672–1674 (2017).
- 27. R. W. Boyd and J. Love, Nonlinear Optics (Elsevier, AP Academic Press, London, 2020), Fourth edition.
- O. Gayer, Z. Sacks, E. Galun, et al., "Temperature and wavelength dependent refractive index equations for MgO-doped congruent and stoichiometric LiNbO₃," Appl. Phys. B 91(2), 343–348 (2008).
- J. S. Pelc, C. R. Phillips, D. Chang, et al., "Efficiency pedestal in quasi-phase-matching devices with random duty-cycle errors," Opt. Lett. 36(6), 864–866 (2011).
- A. K. Hansen, P. E. Andersen, O. B. Jensen, et al., "Highly efficient single-pass sum frequency generation by cascaded nonlinear crystals," Opt. Lett. 40(23), 5526 (2015).
- 31. J. S. Pelc, L. Ma, C. R. Phillips, *et al.*, "Long-wavelength-pumped upconversion single-photon detector at 1550 nm: performance and noise analysis," Opt. Express **19**(22), 21445 (2011).
- 32. L. Meng, A. Padhye, C. Pedersen, *et al.*, "SHG (532 nm)-induced spontaneous parametric downconversion noise in 1064-nm-pumped IR upconversion detectors," Opt. Lett. **44**(7), 1670–1673 (2019).
- J. Titchener, D. Millington-Smith, C. Goldsack, et al., "Single photon lidar gas imagers for practical and widespread continuous methane monitoring," Appl. Energy 306, 118086 (2022).

- L. Rothman, I. Gordon, Y. Babikov, et al., "The hitran2012 molecular spectroscopic database," J. Quant. Spectrosc. Radiat. Transfer 130, 4–50 (2013).
- 35. C. Yu, Q. Xu, and J. Zhang, "Recent advances in InGaAs/InP single-photon detectors," Meas. Sci. Technol. 35(12), 122003 (2024).
- ID Quantique, "ID Qube ULN Detection module," https://www.idquantique.com/quantum-detectionsystems/products/id-qube-uln..
- 37. H. Han, K. Wu, K. Guo, *et al.*, "All-fiber IPDA lidar for CH₄ leakage monitoring using InGaAs/InP single-photon detector," Opt. Express **32**(21), 37155–37166 (2024).
- 38. Excelitas Technologies Corp., "Excelitas SPCM-AQRH," https://www.excelitas.com/product/spcm-aqrh...
- 39. A. Barh, P. J. Rodrigo, L. Meng, *et al.*, "Parametric upconversion imaging and its applications," Adv. Opt. Photonics 11(4), 952–1019 (2019).
- H. Pan and H. Zeng, "Efficient and stable single-photon counting at 155 μm by intracavity frequency upconversion," Opt. Lett. 31(6), 793–795 (2006).
- 41. W. Kang, B. Li, Y. Liang, *et al.*, "Coincidence-Pumping Upconversion Detector Based on Passively Synchronized Fiber Laser System," IEEE Photonics Technol. Lett. **32**(4), 184–187 (2020).
- 42. N. Yao, Q. Yao, X.-P. Xie, *et al.*, "Optimizing up-conversion single-photon detectors for quantum key distribution," Opt. Express **28**(17), 25123–25133 (2020).
- 43. M. Mancinelli, A. Trenti, S. Piccione, *et al.*, "Mid-infrared coincidence measurements on twin photons at room temperature," Nat. Commun. **8**(1), 15184 (2017).
- 44. S. Jiang, K. Huang, T. Yu, *et al.*, "High-resolution mid-infrared single-photon upconversion ranging," Photonics Res. **12**(6), 1294–1302 (2024).
- 45. M. G. Vazimali and S. Fathpour, "Applications of thin-film lithium niobate in nonlinear integrated photonics," Adv. Photonics 4(03), 034001 (2022).
- 46. F. Ma, L.-Y. Liang, J.-P. Chen, et al., "Upconversion single-photon detectors based on integrated periodically poled lithium niobate waveguides [Invited]," J. Opt. Soc. Am. B 35(9), 2096–2101 (2018).
- L. Meng, L. Høgstedt, P. Tidemand-Lichtenberg, et al., "Enhancing the detectivity of an upconversion single-photon detector by spatial filtering of upconverted parametric fluorescence," Opt. Express 26(19), 24712–24722 (2018).